ACS Medicinal Chemistry Letters

pubs.acs.org/acsmedchemlett Letter

Accelerated Discovery of Macrocyclic CDK2 Inhibitor QR-6401 by Generative Models and Structure-Based Drug Design

Yang Yu,*,‡ Junhong Huang,‡ Hu He,‡ Jing Han,‡ Geyan Ye, Tingyang Xu, Xianqiang Sun, Xiumei Chen, Xiaoming Ren, Chunlai Li, Huijuan Li, Wei Huang, Yangyang Liu, Xinjuan Wang, Yongzhi Gao, Nianhe Cheng, Na Guo, Xibo Chen, Jianxia Feng, Yuxia Hua, Chong Liu, Guoyun Zhu, Zhi Xie, Lili Yao, Wenge Zhong, Xinde Chen, Wei Liu, and Hailong Li*

Cite This: https://doi.org/10.1021/acsmedchemlett.2c00515 Read Online

ABSTRACT: Selective CDK2 inhibitors have the potential to provide e□ective therapeutics for CDK2-dependent cancers and for combating drug resistance due to high cyclin E1 (CCNE1) expression intrinsically or CCNE1 amplification induced by treatment of CDK4/6 inhibitors. Generative models that take advantage of deep learning are being increasingly integrated into early drug discovery for hit identification and lead optimization. Here we report the discovery of a highly potent and selective macrocyclic CDK2 inhibitor QR-6401 (**23**) accelerated by the application of generative models and structure-based drug design (SBDD). QR-6401 (**23**) demonstrated robust antitumor e□cacy in an OVCAR3 ovarian cancer xenograft model via oral administration.

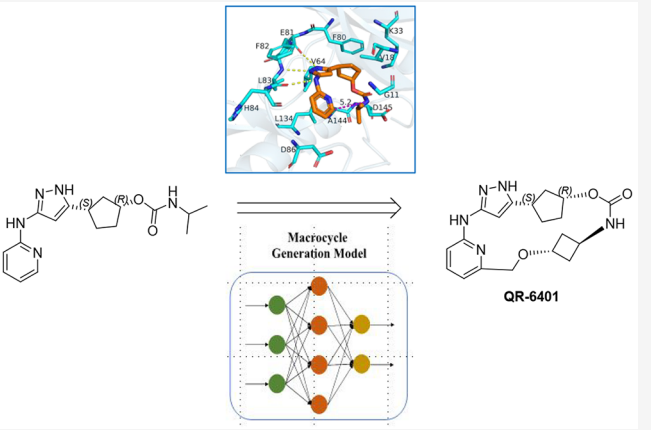

KEYWORDS: *ovarian cancer, CDK2 inhibitor, macrocycle, generative models, SBDD*

The Cyclin-dependent Kinases (CDKs) are a family of serine-threonine kinases which exert their biological functions by interacting with their corresponding cyclin partners.[1] Deregulation of the CDK-cyclin complex's activity results in the loss of cell cycle and transcription control in tumor cells.[2] CDK inhibitors have been pursued by scientists in the pharmaceutical industry for nearly three decades but with limited success. To date only selective dual CDK4/6 inhibitors have been approved for cancer patients, and more selective inhibitors targeting other isoforms of the CDK family are needed.[3,4] The other important CDK isoform that phosphorylates retinoblastoma (Rb) to release E2 transcription factors (E2Fs) in sequence with CDK4/6 is CDK2. CDK2 drives G1/S progression with its canonical binding partner cyclin E1 (CCNE1) whose amplification has been observed in many cancer types and correlates with poorer overall survival rate in breast, ovarian, and other cancer patients.[5,6] Additionally, selective CDK2 inhibitors have the potential to benefit cancer patients who have su□ered drug resistances to CDK4/6 inhibitor treatments due to cyclin E1 amplification.[7] So far only a limited number of selective CDK2 inhibitors are active in clinical trials[8] (Figure 1). After having identified and advanced our next-generation selective CDK2/4/6 inhibitor RGT-419B into development for phase I clinical trial, we initiated an AI-integrated campaign to discover selective CDK2 inhibitors.

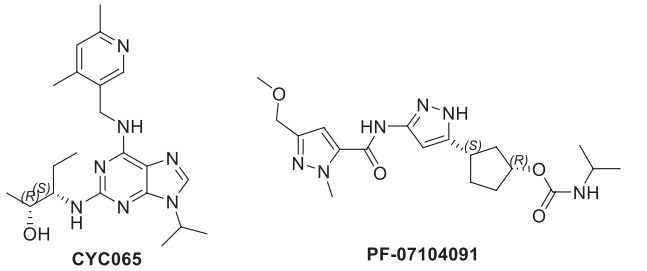

Figure 1. Selected CDK2 inhibitors currently in clinical trials.

Artificial intelligence (AI) in small molecule drug discovery has gained increasing momentum in the past few years.[9,10] The usefulness of AI in drug discovery is demonstrated with several

Received: December 8, 2022
Accepted: January 19, 2023

AI-enabled drug candidates advancing into clinical development.[11] Generally, in order to identify hits with structural novelty and potency, four main types of molecule generation methods are commonly used: scaold (or fragment) hopping, fragment merging, fragment growing, and fragment linking.[12] Each of these methods can be realized through the simplified molecular input line entry system (SMILES) based or graph based generative models[13,14] with the advancements in both algorithm and computing capacity. Recently, we and others have successfully developed generative models for fragment hopping[15,16] and fragment growing.[17−21] Very interestingly, new generative algorithms have demonstrated their capabilities in linking fragments together to form fully elaborated molecules.[22−27]

Macrocycles have emerged successfully as a robust class of modality in small molecule drug discovery.[28,29] Increasing numbers of rationally designed macrocycles by chemists have progressed into clinical trials, and several macrocyclic inhibitors of kinases ALK/ROS1[30] and JAK2/FLT3[31] have been approved as cancer treatments. Conceptually, one can imagine that the fragment linking strategy in FBDD can also be applied intramolecularly to form a macrocyclic molecule from the corresponding linear precursor. Rule-based computational models have been reported for macrocycles construction.[32] AI-based intermolecular linker design algorithms have been published,[22−27] but they cannot be directly applied intramolecularly for macrocycle generation. Pioneering research using AI method to design macrocyclic peptides with much improved permeability has been published by the Baker group very recently.[33] Despite these initial successes and the great potential of this new class of modality, currently no AI algorithms are publicly available for designing such types of molecules with experimental validation in real world drug discovery. Herein we report the AI-accelerated identification of a potent, selective, and orally bioavailable macrocyclic CDK2 inhibitor QR-6401 (**23**).

At the outset of the project, we surveyed the literature and selected 10 representative chemotypes of published CDK2-related inhibitors as possible starting points for us to identify CDK2 inhibitors (Table S1). At the same time a Fragment-Based Variational Auto-Encoder generative model (FBVAE, whose algorithm is to be published elsewhere) was developed to perform fragment hopping of selected starting points. Finally, the essential hinge binding elements of the reference compounds were replaced and a library of 3220 molecules was generated. The inhibitors were filtered through glide docking and visual selection, and finally 10 compounds were prioritized. Some modifications on the generated structures were made for ease of synthesis. These FBVAE-derived analogues were assayed for CDK1/2 inhibitory activities and the results are summarized in Table 1 (Compounds **1**−**10**).

CDK2 inhibitory activities for the synthesized compounds varied widely. While most of them exhibited significantly reduced potencies when compared with their parent molecules (Table S1), compound **10** displayed single digit nanomolar activity with 25-fold CDK1 selectivity. Subsequent SAR exploration around compound **10** was carried out, and we observed that CDK1 selectivity was dicult to improve further and the compounds of the series were cleared rapidly in liver microsomes. On the basis of the early results, we decided to shift our attention toward the fragment replacement of aminopyrazole type of CDK2 inhibitor (Figure 1). Three compounds were selected and synthesized from the 492 generated molecules, and their CDK1/2 inhibitory activities were listed in Table 1 (Compounds **11**−**13**). Overall,

Table 1. Structures and Biological Activities of Novel Compounds Generated by FBVAE

Compound	CDK2/E1 IC_{50} (μM)	CDK1/A2 IC_{50} (μM)	CDK1/CDK2
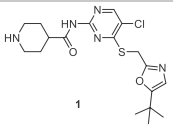 1	8.0	> 50	N/A
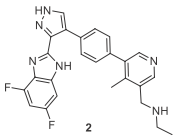 2	> 50	> 50	N/A
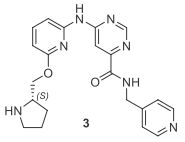 3	> 50	> 50	N/A
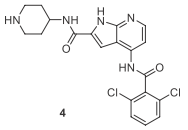 4	> 50	> 50	N/A
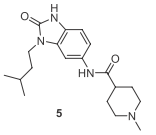 5	> 50	> 50	N/A
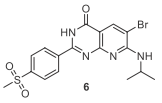 6	5.2	> 17	N/A
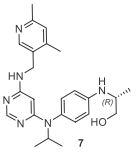 7	> 50	> 50	N/A
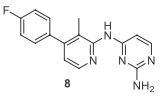 8	1.5	30	20
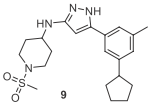 9	> 50	> 50	N/A
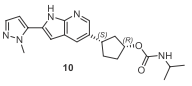 10	0.0015	0.038	25
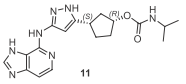 11	0.045	2.5	57
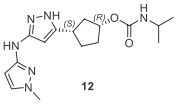 12	0.051	2.7	53
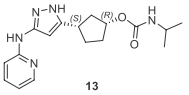 13	0.0081	0.55	67

https://doi.org/10.1021/acsmedchemlett.2c00515
ACS Med. Chem. Lett. XXXX, XXX, XXX−XXX

compound **13** showed better CDK2 activity in enzyme assay and better CDK1 selectivity than compounds **11** and **12**.

In order to gain structural insights for macrocyclic CDK2 inhibitors design, we solved the cocrystal structure of compound **13** with CDK2/Cyclin E1 at 3.0 Å resolution. As illustrated in Figure 2, the aminopyrazole moiety of compound

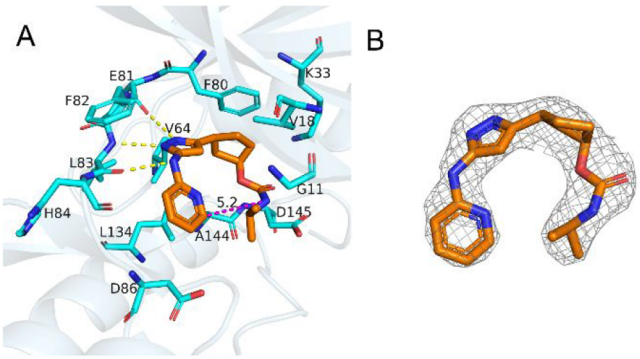

Figure 2. (A) Binding poses of compound **13** with CDK2/Cyclin E1 (PDB: 8H6T). Hydrogen bonds to the backbone atoms of the hinge region are depicted with yellow dashes. (B) 2Fo-Fc electron density map contoured at 1 sigma around the compound in gray mesh.

13 formed the canonical hydrogen bonds with the NH and carbonyl of Leu83 and additional hydrogen bond to backbone carbonyl of Glu81, respectively. The cis-oriented cyclopentyl ring was engaged in van der Waals interactions with the side chain phenyl of gatekeeper residue Phe80. The cocrystal structure also suggested that the carbonyl oxygen from the carbamate motif served as a hydrogen bond acceptor for the side chain amino group of Lys33, while the NH of the carbamate was involved in a hydrogen bond with the side chain carboxyl group of Asp145. The pyridine ring of compound **13** pointed to the solvent-exposed area and showed no obvious polar or nonpolar interactions with the CDK2 protein. Overall, compound **13** adopted a U-shaped binding mode with the 6-position carbon of the pyridine ring and the nitrogen atom of the carbamate motif facing each other. The through-space distance between the two atoms is measured at 5.2 Å, providing rational connecting points for macrocyclization.

A three-step macrocycle generation workflow was envisioned as shown in Figure 3. First, a given starting linear molecule decorated with two preferred attachment points was taken as an input. Then the linkers with preset lengths and chemotypes were generated by MacroTransformer. Finally, they were installed onto the linear molecule by RDKit (an open-source toolkit for cheminformatics) to form a complete macrocycle. MacroTransformer is a novel generative model that was developed for the generation of macrocycles from linear precursors based on the Transformer architecture.[34,35] Known macrocyclic molecules were too few for model training. Thus, acyclic molecules from ChEMBL database were used as training data for data augmentation based on the assumption that a linker fragment could be sliced from an acyclic molecule. The data from the ChEMBL database was filtered by Lipinski's Rules of Five, leaving 456,000 data points. Then the MMPs (matched molecular pairs) algorithm[36] was employed to fragmentize molecules into terminal fragments and linker fragments with 2−15 atoms in length. After removing the duplicated linker fragments, a data set of 123,879 < terminal fragment, linker fragment> pairs were obtained and divided into training set, validation set, and test set by the ratio of 8:1:1. The generative model was trained and evaluated using the ChEMBL data set prepared above. The validity, uniqueness, and novelty of the linkers[37] generated by MacroTransformer were 92%, 84%, and 71%, respectively, indicating that the linkers generated by the model were both valid and novel.

The model was applied to the CDK2 macrocyclic inhibitor design. The preliminary SAR study of the linker length on compound **13** was carried out by medicinal chemists using structure-based drug design. We therefore confined the linker to 4−6 atoms but the chemical nature of the linker was not fixed. The connecting points of the linker were fixed to the 6-position carbon of the pyridine ring and the nitrogen atom of

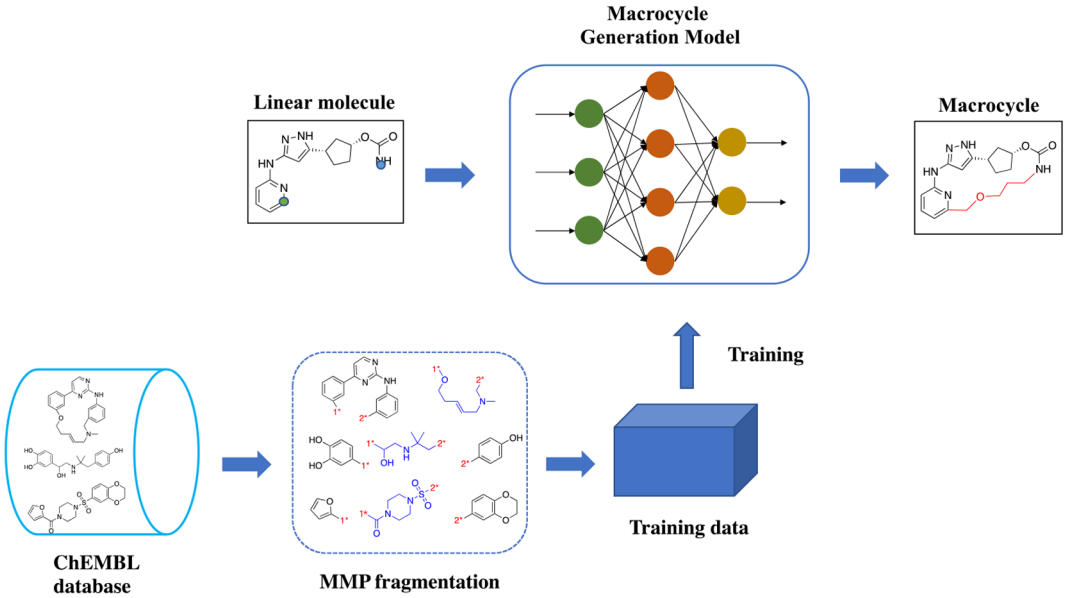

Figure 3. Macrocycle generation pipeline and model construction.

https://doi.org/10.1021/acsmedchemlett.2c00515
ACS Med. Chem. Lett. XXXX, XXX, XXX−XXX

Table 2. Macrocycles Generated by MacroTransformer and Their Biological Activities and Some ADME Properties

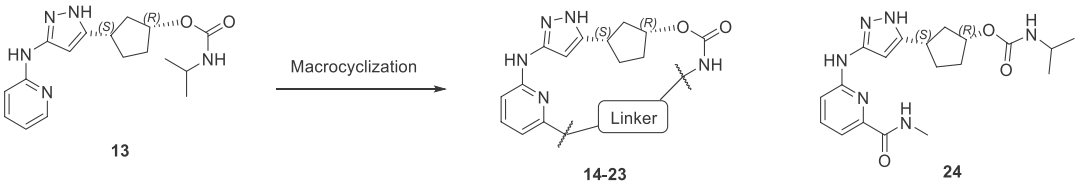

Compound	Linker	CDK2/E1 IC_{50} (nM)	CDK1/A2 IC_{50} (nM)	CDK1/CDK2	OVCAR3 cell IC_{50} (nM)	Human liver microsomal stability $T_{1/2}$ (min)	Permeability: Papp A to B (1E-6 cm/s) /Efflux Ratio
14		0.075	1.25	17	8.7	N/A	N/A
15	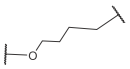	0.18	0.73	4.0	82	12	N/A
16	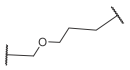	0.41	10	26	30	36	4.5/10
17	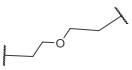	0.92	26	27	58	31	8.6/4.8
18	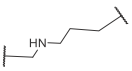	0.26	3.5	13	8.9	N/A	N/A
19	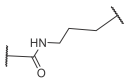	0.090	4.4	48	10	64	0.9/13
20	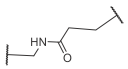	5.1	117	23	411	N/A	N/A
21	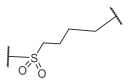	0.051	0.34	6.6	3.2	N/A	N/A
22	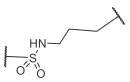	0.053	0.23	4.3	2.6	N/A	N/A
23 (QR-6401)	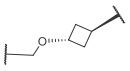	0.37	22	59	34	150	3.2/13
24	N/A	39	1000	26	N/A	N/A	N/A

the carbamate motif in compound **13**. With these being set, compound **13** with two preferred attachment points was used as the starting linear molecule and a total of 7626 macrocycles were generated by MacroTransformer. Then, a field-point score screening[38,39] was performed to check the remaining 7092 compounds to make sure the compounds were in similar 3D pharmacophore with compound **13**, and this process resulted in 978 compounds whose field-point scores were higher than 0.65. Next, glide docking was carried out based on the grid of compound **13** to give 792 compounds of 30 clusters from which medicinal chemists conducted final visual examination. Taking into consideration of structural novelty, drug-likeness, and macrocycle synthesis feasibility, 10 macrocycles were selected and synthesized. The CDK1/2 enzymatic and cellular activities as well as their ADME properties were profiled and summarized in Table 2.

As demonstrated in Table 2, macrocycles with different kinds of linkers generally exhibited 10-fold potency improvement against CDK2 than the acyclic molecule compound **13** except for compound **20**. Especially noteworthy was that compounds **14**, **19**, **21**, and **22** displayed extremely potent subnanomolar CDK2 activities and a single-digit nanomolar antiproliferation effect in ovarian cancer OVCAR3 cells. However, the selectivity against CDK1 varied greatly among the macrocycles, and only analogue **19** exhibited CDK1 selectivity comparable to the starting molecule **13**. The impressive CDK1 selectivity of compound **19** inspired us to obtain its cocrystal structure with CDK2/Cyclin E1, which was

https://doi.org/10.1021/acsmedchemlett.2c00515
ACS Med. Chem. Lett. XXXX, XXX, XXX−XXX

solved at 2.4 Å resolution (Figure 4). The water-mediated hydrogen bond interactions in compound **19** with CDK2/

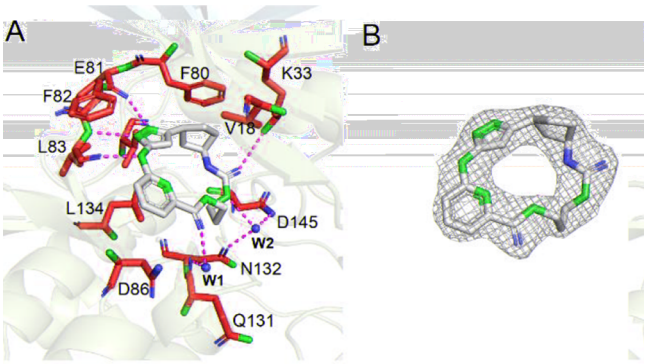

Figure 4. (A) Binding poses of compound **19** with CDK2/Cyclin E1 (PDB: 8H6P). Hydrogen bonds to the backbone atoms of the hinge region are depicted with yellow dashes. W1 and W2 represent the two water molecules involved in mediating H-bond networks between compound **19** and CDK2. (B) 2Fo-Fc electron density map contoured at 1 sigma around the compound in gray mesh.

Cyclin E1 became clearer than those of compound **13** with CDK2/Cyclin E1. The observed binding conformation of compound **19** is in excellent agreement with one of the two computationally calculated minimum conformations (Figure 4 vs Figure S1). Meanwhile, the corresponding acyclic compound **24** was also prepared, tested, and showed much lower CDK2 potency. These results highlighted the importance of the rigid amide linker to lock it into the bioactive binding conformation thus preorganizing the molecule for CDK2 binding with high a□nity. In addition, we tested kinome selectivity of compound **19** in a panel of 330 kinases at 0.1 μM concentration. Compound **19** mainly a□ected CDK and GSK kinases of CMGC family, otherwise it is a quite selective kinase inhibitor (Figure S2).

However, compound **19** su□ered from relatively poor permeability and high e□ux as measured in MDCK cell lines transfected with human MDR1 (Table 2). More linker optimization of compound **16** was carried out by medicinal chemists on the assumption that reducing total polar surface areas of the linker may maintain potency, selectivity, microsomal stability, and improve permeability at the same time. Eventually QR-6401 (**23**) with a trans-cyclobutyl ring as a main part of the linker was identified and achieved the same range potency against CDK2 and OVCAR3 cells with improved human liver microsomal stability and permeability (Table 2). Additionally, this molecule exhibited good selectivity against other closely related kinases, such as CDK1, CDK4, CDK6, CDK9 and GSK3β (Table 3). Furthermore, QR-6401 (**23**) demonstrated good intrinsic metabolic stability and acceptable plasma protein binding in di□erent species (Table 3). The rat and mouse pharmacokinetics studies were conducted, and data were summarized in Table S2 and Table S3. QR-6401 (**23**) was cleared rapidly in SD rat with moderate volume distribution and achieved 50% oral bioavailability at 5 mg/kg. In female Balb/c nude mice, QR-6401 (**23**) displayed superproportional increase of AUC from 758 to 5587 h·ng/mL following PO dose at 20 and 100 mg/kg, presumably due to a certain level of saturation of clearance.

On the basis of the overall potency, selectivity, ADME and PK profile of QR-6401 (**23**), it was advanced into *in vivo* antitumor e□cacy study in OVCAR3 ovarian cancer xenograft model. Tumor-bearing mice were dosed with QR-6401 (**23**) twice daily through oral gavage at 50 mg/kg for 28 days. Free plasma concentrations at this dose allowed about 12 h coverage over the cellular IC_{50} of QR-6401 (**23**) (Figure S5). Treatment with QR-6401 (**23**) caused significant tumor growth inhibition (TGI% = 78%, Figure 5A) in the OVCAR3 xenograft model. QR-6401 (**23**) was well tolerated, and no apparent body weight loss was observed when compared to the vehicle group (Figure 5B). To elucidate the mechanism of antitumor activity, we examined the pharmacodynamic response to QR-6401 (**23**) treatment in the OVCAR3 ovarian cancer xenografts model. QR-6401 (**23**) was administered twice daily via oral gavage at 50 mg/kg to OVCAR3 tumor-bearing mice with 6 h apart between AM and PM dosing time. Tumors were collected at defined time points 3 days post treatment and the levels of retinoblastoma (Rb) phosphorylation at serine 807/811 were determined. QR-6401 (**23**) produced robust suppression of Rb phosphorylation, and 80%, 69% and 73% inhibition were observed at 2, 4, and 7 h post first dose at day 3, respectively, when compared to the vehicle control (Figure 5C and 5D). Free plasma concentrations at 2, 4, and 7 h were 33, 20, and 51 nM, respectively (Figure 5D).

In summary, we report herein the accelerated discovery of a potent, selective, and orally bioavailable macrocyclic CDK2 inhibitor QR-6401 (**23**). During our e□ort, new AI methods of generative models were developed, evaluated, and deeply integrated into hit identification and lead optimization stages. At the early stage of the project, the sca□old hopping model FBVAE was used to produce a novel and proprietary lead CDK2 compound **10** from publicly disclosed CDK inhibitors for further optimization. Then a macrocyclization strategy was envisioned on the basis of the cocrystal structure of compound **13** with CDK2/Cyclin E1. And at the lead optimization stage, the macrocycle generative model MacroTransformer was developed and utilized in the linker design. The AI model generated extremely potent CDK2 macrocyclic inhibitors with excellent CDK1 selectivity. However, it is important to point out that these molecules were also conceived by our internal chemist. In fairness, the model performed well if not better than human intelligence in our case. Perhaps more importantly, QR-6401 (**23**) was not produced by the MacroTransformer model but by our experienced chemists, highlighting the notion that AI generative models in general and MacroTransformer in particular are still in early development stages. Possible future directions for algorithm evolution are to expand structural diversity with more chemotypes and

Table 3. In Vitro Profile of QR-6401 (23)

Biochemical activity IC_{50} (nM)						Plasma protein binding in 100% plasma			Liver microsomal stability $T_{1/2}$ (min)		
CDK1/A2	CDK2/E1	CDK4/D1	CDK6/D3	CDK9/T1	GSK3β	mouse	rat	human	mouse	rat	dog
22	0.37	45	34	10	5.5	79%	70%	99%	68	150	100

https://doi.org/10.1021/acsmedchemlett.2c00515
ACS Med. Chem. Lett. XXXX, XXX, XXX−XXX

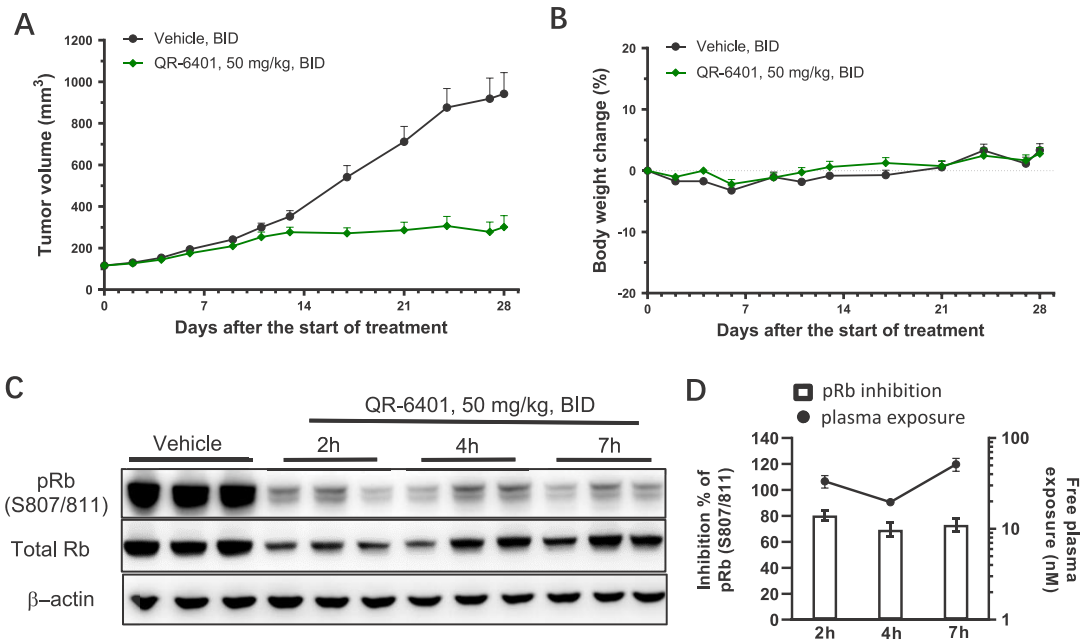

Figure 5. QR-6401 (**23**) demonstrated robust antitumor activity in OVCAR3 xenograft model. (A) In vivo tumor growth inhibition of QR-6401 (**23**) in OVCAR3 ovarian cancer xenograft. (B) Body weight change in OVCAR3 xenograft. (C) Pharmacodynamic inhibition. (D) Inhibition of Rb phosphorylation and corresponding plasma exposure. Inhibition of pRb (S807/811) compared to vehicle control was calculated after normalization to β-actin. Vehicle: 20% PEG400, 10% Solutol HS15, 70% (0.5% Methyl cellulosein deionized water) solution.

take 3-dimensional structural information on linkers and target proteins into consideration. In this project, generative model engineers, computational chemists and medicinal chemists worked seamlessly together and inspired each other in new inhibitor design and optimization, which greatly accelerated the discovery process and resulted in the identification of an advanced lead macrocycle QR-6401 (**23**).

ASSOCIATED CONTENT

Supporting Information

The Supporting Information is available free of charge at https://pubs.acs.org/doi/10.1021/acsmedchemlett.2c00515.

Computational methods, synthetic procedures, characterization of final compounds, protocols of *in intro* and *in vivo* assays, kinome selectivity data, protocols and results of ADME and PK studies, protocols of OVCAR3 xenograft and PK/PD studies, copies of NMR spectra (PDF)

Compound lists generated by FBVAE and MacroTransformer (XLSX)

AUTHOR INFORMATION

Corresponding Authors

Yang Yu – *Tencent AI Lab, Tencent, Shenzhen 518057, China;* orcid.org/0000-0003-2125-3229; Email: kevin_yu1985@hotmail.com

Hailong Li – *Regor Therapeutics Group, Shanghai 201210, China;* orcid.org/0000-0002-6021-9448; Email: hailong.li@qlregor.com

Authors

Junhong Huang – *Tencent AI Lab, Tencent, Shenzhen 518057, China*

Hu He – *Regor Therapeutics Group, Shanghai 201210, China;* Present Address: Synrx Therapeutics (Hangzhou) CO., Ltd., Zhejiang, 311121, China

Jing Han – *Regor Therapeutics Group, Shanghai 201210, China*

Geyan Ye – *Tencent AI Lab, Tencent, Shenzhen 518057, China*

Tingyang Xu – *Tencent AI Lab, Tencent, Shenzhen 518057, China*

Xianqiang Sun – *Regor Therapeutics Group, Shanghai 201210, China;* Present Address: AutoDrug Biotech Co. Ltd., Shanghai, 201210, China

Xiumei Chen – *Regor Therapeutics Group, Shanghai 201210, China*

Xiaoming Ren – *Regor Therapeutics Group, Shanghai 201210, China*

Chunlai Li – *Regor Therapeutics Group, Shanghai 201210, China*

Huijuan Li – *Regor Therapeutics Group, Shanghai 201210, China*

Wei Huang – *Regor Therapeutics Group, Shanghai 201210, China;* Present Address: Structure Therapeutics, Shanghai, 201203, China

Yangyang Liu – *Regor Therapeutics Group, Shanghai 201210, China*

Xinjuan Wang – *Regor Therapeutics Group, Shanghai 201210, China*

Yongzhi Gao – *Regor Therapeutics Group, Shanghai 201210, China*

Nianhe Cheng – *Regor Therapeutics Group, Shanghai 201210, China*

Na Guo – *BioDuro-Sundia, Shanghai 200131, China*

Xibo Chen – *BioDuro-Sundia, Shanghai 200131, China*

Jianxia Feng – *BioDuro-Sundia, Beijing 102200, China*

Yuxia Hua – *BioDuro-Sundia, Beijing 102200, China*

Chong Liu – *BioDuro-Sundia, Beijing 102200, China*
Guoyun Zhu – *Regor Therapeutics Group, Shanghai 201210, China*
Zhi Xie – *Regor Therapeutics Group, Shanghai 201210, China*
Lili Yao – *Regor Therapeutics Group, Shanghai 201210, China*
Wenge Zhong – *Regor Therapeutics Group, Shanghai 201210, China*
Xinde Chen – *Tencent AI Lab, Tencent, Shenzhen 518057, China*
Wei Liu – *Tencent AI Lab, Tencent, Shenzhen 518057, China*

Complete contact information is available at:
https://pubs.acs.org/10.1021/acsmedchemlett.2c00515

Author Contributions

‡Y.Y., J.H., H.H., and J.H. contributed equally.

Notes

The authors declare no competing financial interest.

ACKNOWLEDGMENTS

The authors would like to thank Drs. Jing Lin and Xiaotian Zhu at Regor Therapeutics Group for scientific discussion during the research, Xi Chen and Yanny Nie at Regor Therapeutics Group for project management support, and Dr. Jian Shen at Viva Biotech for protein reagents and co-crystallization. The X-ray di□raction experiment in this work was carried out with the support of Shanghai Synchrotron Radiation Facility, Beamline BL02U1.

ABBREVIATIONS

CDK, cyclin-dependent kinase; CCNE1, cyclin E1; AI, artificial intelligence; ADME, absorption, distribution, metabolism, and elimination; FBDD, fragment-based drug discovery; ALK, anaplastic lymphoma kinase; ROS1, c-ros oncogene 1; JAK2, Janus kinase 2; FLT3, fms-like tyrosine kinase 3; OVCAR3, human epithelial ovarian adenocarcinoma; FBVAE, fragment-based variational autoencoder generative model; MDCK, Madin-Darby canine kidney; GSK3β, glycogen synthase kinase 3 beta; PO, per oral; AUC, area under the drug concentration–time curve; TGI, tumor growth inhibition; PK, pharmacokinetic properties; FBVAE, Fragment-Based Variational Auto-Encoder generative model; Graph-GMVAE, Graph-Based Variational Auto-Encoder; Macro-Transformer, the name of the macrocyclization algorithm developed by us; RDKit, an open source toolkit for cheminformatics; MMPs, matched molecular pairs

REFERENCES

(1) Malumbres, M. Cyclin-dependent kinases. *Genome Biol.* **2014**, *15* (6), 122.
(2) Schwartz, G. K.; Shah, M. A. Targeting the Cell Cycle: A New Approach to Cancer Therapy. *J. Clin. Oncol.* **2005**, *23* (36), 9408–9421.
(3) Yuan, K.; Wang, X.; Dong, H.; Min, W.; Hao, H.; Yang, P. Selective inhibition of CDK4/6: A safe and effective strategy for developing anticancer drugs. *Acta Pharm. Sin. B* **2021**, *11* (1), 30–54.
(4) Jhaveri, K.; Burris, H. A., III; Yap, T. A.; Hamilton, E.; Rugo, H. S.; Goldman, J. W.; Dann, S.; Liu, F.; Wong, G. Y.; Krupka, H.; Shapiro, G. I. The evolution of cyclin dependent kinase inhibitors in the treatment of cancer. *Expert Rev. Anticancer Ther.* **2021**, *21* (10), 1105–1124.
(5) Tadesse, S.; Caldon, E. C.; Tilley, W.; Wang, S. Cyclin-Dependent Kinase 2 Inhibitors in Cancer Therapy: An Update. *J. Med. Chem.* **2019**, *62* (9), 4233–4251.
(6) Sokolsky, A.; Winterton, S.; Kennedy, K.; Drake, K.; Stump, K.; Huo, L.; Lo, Y.; Ye, M.; Covington, M.; Diamond, S.; Yang, Y.-o.; Kim, S.; Yeleswaram, S.; Wu, L.; Yao, W. Discovery of 5,7-Dihydro-6H-pyrrolo[2,3-d]pyrimidin-6-ones as Highly Selective CDK2 Inhibitors. *ACS Med. Chem. Lett.* **2022**, *13* (11), 1797–1804.
(7) Herrera-Abreu, M. T.; Palafox, M.; Asghar, U.; Rivas, M. A.; Cutts, R. J.; Garcia-Murillas, I.; Pearson, A.; Guzman, M.; Rodriguez, O.; Grueso, J.; Bellet, M.; Cortés, J.; Elliott, R.; Pancholi, S.; Lord, C. J.; Baselga, J.; Dowsett, M.; Martin, L.-A.; Turner, N. C.; Serra, V. Early Adaptation and Acquired Resistance to CDK4/6 Inhibition in Estrogen Receptor-Positive Breast Cancer. *Cancer Res.* **2016**, *76* (8), 2301–2313.
(8) Details of these trials can be found at https://clinicaltrials.gov/ct2/results?cond=CDK2&recrs=a&recrs=d&age_v=&gndr=&type=&rslt=&Search=Apply. (accessed Jan 15, 2023).
(9) Vijayan, R. S. K.; Kihlberg, J.; Cross, J. B.; Poongavanam, V. Enhancing preclinical drug discovery with artificial intelligence. *Drug Discovery Today* **2022**, *27* (4), 967–984.
(10) Jayatunga, M. K. P.; Xie, W.; Ruder, L.; Schulze, U.; Meier, C. AI in small-molecule drug discovery: a coming wave? *Nat. Rev. Drug Discovery* **2022**, *21*, 175–176.
(11) Kirkpatrick, P. Artificial intelligence makes a splash in small-molecule drug discovery*Biopharm. Deal.* **2022** DOI: 10.1038/d43747-022-00104-7.
(12) Erlanson, D. A.; Fesik, S. W.; Hubbard, R. E.; Jahnke, W.; Jhoti, H. Twenty years on: the impact of fragments on drug discovery. *Nat. Rev. Drug Discovery* **2016**, *15* (9), 605–619.
(13) Vanhaelen, Q.; Lin, Y.-C.; Zhavoronkov, A. The Advent of Generative Chemistry. *ACS Med. Chem. Lett.* **2020**, *11* (8), 1496–1505.
(14) Tong, X.; Liu, X.; Tan, X.; Li, X.; Jiang, J.; Xiong, Z.; Xu, T.; Jiang, H.; Qiao, N.; Zheng, M. Generative Models for De Novo Drug Design. *J. Med. Chem.* **2021**, *64* (19), 14011–14027.
(15) Yu, Y.; Xu, T.; Li, J.; Qiu, Y.; Rong, Y.; Gong, Z.; Cheng, X.; Dong, L.; Liu, W.; Li, J.; Dou, D.; Huang, J. A Novel Scalarized Scaffold Hopping Algorithm with Graph-Based Variational Autoencoder for Discovery of JAK1 Inhibitors. *ACS Omega* **2021**, *6* (35), 22945–22954.
(16) Bos, P. H.; Houang, E. M.; Ranalli, F.; Leffler, A. E.; Boyles, N. A.; Eyrich, V. A.; Luria, Y.; Katz, D.; Tang, H.; Abel, R.; Bhat, S. AutoDesigner, a De Novo Design Algorithm for Rapidly Exploring Large Chemical Space for Lead Optimization: Application to the Design and Synthesis of d-Amino Acid Oxidase Inhibitors. *J. Chem. Inf. Model.* **2022**, *62* (8), 1905–1915.
(17) Tan, X.; Li, C.; Yang, R.; Zhao, S.; Li, F.; Li, X.; Chen, L.; Wan, X.; Liu, X.; Yang, T.; Tong, X.; Xu, T.; Cui, R.; Jiang, H.; Zhang, S.; Liu, H.; Zheng, M. Discovery of Pyrazolo[3,4-d]pyridazinone Derivatives as Selective DDR1 Inhibitors via Deep Learning Based Design, Synthesis, and Biological Evaluation. *J. Med. Chem.* **2022**, *65* (1), 103–119.
(18) Bagal, V.; Aggarwal, R.; Vinod, P. K.; Priyakumar, U. D. MolGPT: Molecular Generation Using a Transformer-Decoder Model. *J. Chem. Inf. Model.* **2022**, *62* (9), 2064–2076.
(19) Powers, A. S.; Yu, H. H.; Suriana, P.; Dror, R. O. Fragment-Based Ligand Generation Guided By Geometric Deep Learning On Protein-Ligand Structure. *bioRxiv*, March 21, 2022. DOI: 10.1101/2022.03.17.484653.
(20) Chen, H. Can Generative-Model-Based Drug Design Become a New Normal in Drug Discovery? *J. Med. Chem.* **2022**, *65* (1), 100–102.
(21) Fu, T.; Gao, W.; Xiao, C.; Yasonik, J.; Coley, C. W.; Sun, J. Di□erentiable Sca□olding Tree for Molecular Optimization. *arXiv (Machine Learning)*, Jan. 24, 2021, 2109.10469, ver. 1. https://arxiv.org/abs/2109.10469.
(22) Huang, Y.; Peng, X.; Ma, J.; Zhang, M. 3DLinker: An E(3) Equivariant Variational Autoencoder for Molecular Linker Design.

arXiv (Machine Learning), May 15, 2022, 2205.07309. https://arxiv.org/abs/2205.07309.

(23) Igashov, I.; Stärk, H.; Vignac, C.; Satorras, V. G. F.; Pascal; Welling, M.; Bronstein, M.; Correia, B. Equivariant 3D-Conditional Di□usion Models for Molecular Linker Design. *arXiv*, Oct. 11, 2022, 2210.05274, ver. 1. https://arxiv.org/abs/2210.05274.

(24) Tan, Y.; Dai, L.; Huang, W.; Guo, Y.; Zheng, S.; Lei, J.; Chen, H.; Yang, Y. DRlinker: Deep Reinforcement Learning for Optimization in Fragment Linking Design. *J. Chem. Inf. Model.* **2022**, *62*, 5907−5917.

(25) Imrie, F.; Hadfield, T. E.; Bradley, A. R.; Deane, C. M. Deep generative design with 3D pharmacophoric constraints. *Chem. Sci.* **2021**, *12* (43), 14577−14589.

(26) Imrie, F.; Bradley, A. R.; van der Schaar, M.; Deane, C. M. Deep Generative Models for 3D Linker Design. *J. Chem. Inf. Model.* **2020**, *60* (4), 1983−1995.

(27) Yang, Y.; Zheng, S.; Su, S.; Zhao, C.; Xu, J.; Chen, H. SyntaLinker: automatic fragment linking with deep conditional transformer neural networks. *Chem. Sci.* **2020**, *11* (31), 8312−8322.

(28) Cummings, M. D.; Sekharan, S. Structure-Based Macrocycle Design in Small-Molecule Drug Discovery and Simple Metrics To Identify Opportunities for Macrocyclization of Small-Molecule Ligands. *J. Med. Chem.* **2019**, *62* (15), 6843−6853.

(29) Marsault, E.; Peterson, M. L. Macrocycles Are Great Cycles: Applications, Opportunities, and Challenges of Synthetic Macrocycles in Drug Discovery. *J. Med. Chem.* **2011**, *54* (7), 1961−2004.

(30) Johnson, T. W.; Richardson, P. F.; Bailey, S.; Brooun, A.; Burke, B. J.; Collins, M. R.; Cui, J. J.; Deal, J. G.; Deng, Y.-L.; Dinh, D.; Engstrom, L. D.; He, M.; Hoffman, J.; Hoffman, R. L.; Huang, Q.; Kania, R. S.; Kath, J. C.; Lam, H.; Lam, J. L.; Le, P. T.; Lingardo, L.; Liu, W.; McTigue, M.; Palmer, C. L.; Sach, N. W.; Smeal, T.; Smith, G. L.; Stewart, A. E.; Timofeevski, S.; Zhu, H.; Zhu, J.; Zou, H. Y.; Edwards, M. P. Discovery of (10R)-7-Amino-12-fluoro-2,10,16-trimethyl-15-oxo-10,15,16,17-tetrahydro-2H-8,4-(metheno)pyrazolo-[4,3-h][2,5,11]-benzoxadiazacyclotetradecine-3-carbonitrile (PF-06463922), a Macrocyclic Inhibitor of Anaplastic Lymphoma Kinase (ALK) and c-ros Oncogene 1 (ROS1) with Preclinical Brain Exposure and Broad-Spectrum Potency against ALK-Resistant Mutations. *J. Med. Chem.* **2014**, *57* (11), 4720−4744.

(31) William, A. D.; Lee, A. C. H.; Blanchard, S.; Poulsen, A.; Teo, E. L.; Nagaraj, H.; Tan, E.; Chen, D.; Williams, M.; Sun, E. T.; Goh, K. C.; Ong, W. C.; Goh, S. K.; Hart, S.; Jayaraman, R.; Pasha, M. K.; Ethirajulu, K.; Wood, J. M.; Dymock, B. W. Discovery of the Macrocycle 11-(2-Pyrrolidin-1-yl-ethoxy)-14,19-dioxa-5,7,26-triazatetracyclo[19.3.1.1(2,6).1(8,12)]heptacosa-1(25),2(26),3,5,8,10,12(27),16,21,23-decaene (SB1518), a Potent Janus Kinase 2/Fms-Like Tyrosine Kinase-3 (JAK2/FLT3) Inhibitor for the Treatment of Myelofibrosis and Lymphoma. *J. Med. Chem.* **2011**, *54* (13), 4638−4658.

(32) Sindhikara, D.; Wagner, M.; Gkeka, P.; Güssregen, S.; Tiwari, G.; Hessler, G.; Yapici, E.; Li, Z.; Evers, A. Automated Design of Macrocycles for Therapeutic Applications: From Small Molecules to Peptides and Proteins. *J. Med. Chem.* **2020**, *63* (20), 12100−12115.

(33) Bhardwaj, G.; O'Connor, J.; Rettie, S.; Huang, Y.-H.; Ramelot, T. A.; Mulligan, V. K.; Alpkilic, G. G.; Palmer, J.; Bera, A. K.; Bick, M. J.; Di Piazza, M.; Li, X.; Hosseinzadeh, P.; Craven, T. W.; Tejero, R.; Lauko, A.; Choi, R.; Glynn, C.; Dong, L.; Griffin, R.; van Voorhis, W. C.; Rodriguez, J.; Stewart, L.; Montelione, G. T.; Craik, D.; Baker, D. Accurate de novo design of membrane-traversing macrocycles. *Cell* **2022**, *185* (19), 3520−3532.

(34) Vaswani, A.; Shazeer, N.; Parmar, N.; Uszkoreit, J.; Jones, L.; Gomez, A. N.; Kaiser, Ł.; Polosukhin, I. Attention is all you need. *Proceedings of the 31st International Conference on Neural Information Processing Systems*; Long Beach, California, USA, 2017.

(35) Wang, S.; Guo, Y.; Wang, Y.; Sun, H.; Huang, J. SMILES-BERT: Large Scale Unsupervised Pre-Training for Molecular Property Prediction. *Proceedings of the 10th ACM International Conference on Bioinformatics*; Computational Biology and Health Informatics: Niagara Falls, NY, 2019.

(36) Arús-Pous, J.; Patronov, A.; Bjerrum, E. J.; Tyrchan, C.; Reymond, J.-L.; Chen, H.; Engkvist, O. SMILES-based deep generative scaffold decorator for de-novo drug design. *J. Cheminformatics* **2020**, *12* (1), 38.

(37) McNaughton, A. D.; Bontha, M. S.; Knutson, C. R.; Pope, J. A.; Kumar, N. De novo design of protein target specific sca□old-based Inhibitors via Reinforcement Learning. *arXiv*, May 21, 2022, 2205.10473, ver. 1. https://arxiv.org/abs/2205.10473.

(38) Cheeseright, T.; Mackey, M.; Rose, S.; Vinter, A. Molecular Field Extrema as Descriptors of Biological Activity: Definition and Validation. *J. Chem. Inf. Model.* **2006**, *46* (2), 665−676.

(39) Cheeseright, T. J.; Mackey, M. D.; Melville, J. L.; Vinter, J. G. FieldScreen: Virtual Screening Using Molecular Fields. Application to the DUD Data Set. *J. Chem. Inf. Model.* **2008**, *48* (11), 2108−2117.

https://doi.org/10.1021/acsmedchemlett.2c00515
ACS Med. Chem. Lett. XXXX, XXX, XXX−XXX